Local symmetry of nitrogen pairs in GaP

B. Gil, J. Camassel, J. P. Albert, and H. Mathieu
Groupe d'Etude des Semiconducteurs, Université des Sciences et Techniques du Languedoc, F-34060 Montpellier-Cedex, France
(Received 19 July 1985)

We report an investigation of the stress-induced splitting pattern of NN_i pairs in GaP. Analyzing the data in terms of stress-induced components and relative intensities, we deduce the local symmetry of pairs ranging from NN_1 to NN_7. With the exception of NN_1, NN_3, and NN_4, we find results which cannot be directly accounted for in light of the standard assignment for pairs of substitutional nitrogen atoms.

I. INTRODUCTION

Excitons bound to isoelectronic centers have been investigated for about twenty years. The simplest form of isoelectronic centers appears to be neutral defects produced when one atom of a host crystal is substituted by an atom of the same column of the Periodic Table. Examples are oxygen substituting for tellurium in ZnTe (Ref. 1) or nitrogen substituting for phosphorus in GaP (Ref. 2). More complicated defects have also been investigated. They correspond to near-neighbor combinations of neutral defects [for instance, nitrogen-nitrogen pairs in GaP (Ref. 2)] or complex substitutions of atoms which conserve the average number of valence electrons [for instance, four lithium atoms replacing one single silicon atom in silicon (Ref. 3) or three copper atoms replacing one phosphorus in GaP (Ref. 4)]. A common feature to all isoelectronic centers is their very efficient luminescence property. The local impurity potentiai first traps electron-hole pairs which next recombine radiatively. This has long been recognized as a powerful tool in processing indirect band-gap semiconductors and makes, for instance, GaP:N and $Ga_{1-x}As_xP$:N useful materials for light emitting diodes (Ref. 5).

On the theoretical side, the problem is more complex. Since there is no simple Coulomb field to bind an extra particle, the binding mechanism originates, in this case, only from the difference in atomic structure and from lattice-relaxation effects. However, a correct description of the two mechanisms is far from obvious. Consider, for instance, nitrogen substituting for phosphorus. The first contribution makes this substituent appear as a deep (strongly localized) potential well. This was first recognized by Faulkner[6] who, assuming that the bare impurity potential was nothing but the difference of the two pseudopotentials of nitrogen and phosphorus, performed a Slater-Koster calculation. He ended up with a deep bound state for electrons localized about 1 eV inside the forbidden gap, which strongly disagrees with the experimental results. The exciton binding energy is only 11 meV and most experimental findings suggest that N^- should be unstable in GaP.[7-9] In fact, the lattice relaxation partly cancels the nitrogen potential[8] and the binding mechanism of electron-hole pairs can only be understood by taking into account correlation effects.[9,10]

When two nitrogen atoms come into near-neighbor positions, both the elastic and electrostatic parts of the localized potential increase and become anisotropic. The net result of the two mechanisms is to favor the binding of a single electron to pairs of nitrogen atoms, to constitute an isoelectronic acceptor NN^- which next attracts a hole. Such a viewpoint is nothing but the Hopfield-Thomas-Lynch model of excitons bound to isoelectronic centers.[1,2] This simple viewpoint results in two consequences.

(i) The greater the pair separation, the smaller the binding energy. Indeed, GaP:N exhibits a series of isoelectronic traps NN_i whose exciton binding energies range from 140 meV (NN_1) to 11 meV for an isolated nitrogen atom (NN_∞). As a consequence, a straightforward assignment was deduced.[2] It associates NN_1 with two nitrogen atoms in first-neighbor positions on the anionic site, NN_2 with the second-neighbor positions, and so on. This assignment has been widely used in the current literature.[2,6,7,9]

(ii) Whatever the pair index i, the hole being bound by identical Coulomb potentials should exhibit an almost identical series of hydrogenic excited states. Indeed, luminescence excitation spectroscopy[7] reveals that the deep NN_i pairs ($i<7$) all exhibit sharp excited states. The hole binding energies which correspond are 40 meV for NN_1 and 34 meV for NN_7. For shallow NN_i traps ($i>7$), the electrons become more delocalized and the excited states become broader and overlap the free-exciton continuum. Lastly, for isolated nitrogen the electron is not believed to be bound and, as already discussed, both Coulomb and correlation effects are needed to stabilize the electron-hole pair.

In this work we focus on the symmetry properties associated with the pair spectra ranging from NN_1 to NN_7. We apply a uniaxial stress along the [001], [111], and [110] crystallographic directions in order to change, in nonequivalent ways, the near-neighbor distances associated with a given family of defects. Analyzing the stress-induced splitting patterns, we discuss the defect orientation. This is best viewed using a simple example. Consider, for instance, a pair of substitutional atoms lying along a cubic direction. Under application of a $\langle 100 \rangle$ stress, the atoms move closer in one pair and apart in the two others. This results in two different families with respective populations 1 and 2. Under application of a $\langle 111 \rangle$ stress, on the contrary, the threefold degeneracy is not lift-

TABLE I. Local point groups associated with the six possible families of axial defects corresponding to NN pairs in GaP. After application of a uniaxial stress, the crystal symmetry reduces and the spatial degeneracy of equivalent defects is lifted. Results are tabulated for ⟨001⟩, ⟨111⟩, and ⟨110⟩ uniaxial stress.

Orientation of the defect	T_d	$D_{2d}^{\langle 001\rangle}$	$C_{3v}^{\langle 111\rangle}$	$C_{2v}^{\langle 110\rangle}$
$[aa0]$	$4C_{3v}$	$4C_s\{110\}$	$C_{3v}^{\langle 111\rangle}+3C_s\{110\}$	$2C_s\{110\}+2C_s'\{110\}$
[00a]	$3D_{2d}$	$D_{2d}^{\langle 00a\rangle}+2D_2^{\langle a00\rangle}$	$3C_s\{110\}$	$C_{2v}^{\langle 001\rangle}+2E$
$[aa0]$	$6C_{2v}$	$2C_{2v}^{\langle 110\rangle}+4E$	$3C_s\{\bar{1}10\}+3C_s'\{110\}$	$C_{2v}^{\langle 110\rangle}+C_{2v}^{\langle 1\bar{1}0\rangle}+4E$
$[aac]$	$12C_s$	$4C_s\{110\}+8E$	$3C_s^{\{\bar{1}01\}}+3C_s'\{\bar{1}01\}+6E$	$2C_s\{110\}+2C_s\{\bar{1}10\}+4E^{\langle a\bar{b}a\rangle}+4E^{\langle \bar{a}b\bar{a}\rangle}$
$[ab0]$	$12C_2$	$4C_2^{\langle ab0\rangle}+4C_2^{\langle b0a\rangle}+4C_2\langle 0ab\rangle$	$6E^{\langle ab0\rangle}+6E'^{\langle a\bar{b}0\rangle}$	$2C_2^{\langle ab0\rangle}+2C_2'^{\langle \bar{a}b0\rangle}+4E^{\langle ab0\rangle}+4E'^{\langle b0a\rangle}$
$[abc]$	$24E$	$8E^{\langle acb\rangle}+8E^{\langle abc\rangle}+8E^{\langle bca\rangle}$	$6E^{\langle bca\rangle}+6E^{\langle ab\bar{c}\rangle}+6E^{\langle \bar{b}ca\rangle}+6E^{\langle bc\bar{a}\rangle}$	$4E^{\langle abc\rangle}+4E^{\langle a\bar{b}c\rangle}+4E^{\langle bca\rangle}+4E^{\langle b\bar{c}a\rangle}+4E^{\langle acb\rangle}+4E^{\langle a\bar{c}b\rangle}$

ed. Provided the defect symmetry is mainly controlled by the position of the two neighboring atoms in the real crystal, a generalization of these simple ideas to all possible nitrogen positions should permit one to identify unambiguously the physical origin of the deep NN_i pairs ($i<7$).

II. SYMMETRY CONSIDERATIONS

The method we use is an application of the ideas developed independently by Kaplyanskii[11] to investigate noncubic centers in cubic crystals, and by Morgan and Morgan[12] to investigate cadmium-oxygen pairs in GaP. The main difference with the case of Cd-O pairs is that, in this case, both impurities are located on adjacent lattice sites, directed along the ⟨111⟩ directions, and that all defects had C_{3v} symmetry. In the case of nitrogen-nitrogen pairs, the situation is more complicated. The two impurities are located on the same (anion) sublattice and the local symmetry group depends on the orientation of the nitrogen-nitrogen direction with respect to the cubic axes. Working in the set of local symmetry axes defined in Ref. 13, we find only six possible configurations. The local point groups are C_{3v}, D_{2d}, C_s, C_2, and E. Except for E and C_2, all correspond with N-N pairs lying in the {110} planes. The number of equivalent orientations gives an n-branched star of pairs whose degeneracy is lifted by lowering the crystal symmetry.

After inspection of the six families of defects under application of the ⟨001⟩, ⟨111⟩, and ⟨110⟩ uniaxial stress, we get all results listed in Table I. We find only two configurations which conserve the same degeneracy under application of a uniaxial stress: (i) defects of C_{3v} symmetry under application of a ⟨001⟩ stress, and (ii) defects of D_{2d} symmetry under application of a ⟨111⟩ stress. All other configurations split into a number of families which depend on the stress direction.

The case of C_s pairs under ⟨111⟩ stress is interesting to discuss. A ⟨111⟩ stress gives six pairs with very low E symmetry and six pairs with C_s symmetry. The mirror plane in both cases is {101} but the six C_s pairs are not equivalent under the symmetry operations of the strained crystal. This gives two families.

In order to associate one given family with a definite local symmetry, we first discuss the data in terms of relative intensities. Next, we try to be more quantitative and consider the different stress-split families. This is done in the following way. We consider only the deformation experienced along the pair direction and assume that the larger the deformation, the greater the change in binding energy. Let (α,β,γ) be the cosines of a given pair with respect to the set of crystallographic axes, the axial deformation $e_{z'z'}$ is given by

$$e_{z'z'}=\alpha^2e_{xx}+\beta^2e_{yy}+\gamma^2e_{zz}+2(\alpha\beta e_{xy}+\beta\gamma e_{yz}+\gamma\alpha e_{zx}),$$

where the components of the strain tensor in the crystallographic axis depend on the stress direction. For conveni-

TABLE II. Strain components associated with the stress magnitude (X) for all stress directions investigated in this work: $e_H=(S_{11}+2S_{12})X/3$, $e_{001}=(S_{11}-S_{12})X/3$, $e_{111}=S_{44}X/6$.

Stress direction	Strain component e_{xx}	e_{yy}	e_{zz}	e_{xz}	e_{yz}	e_{yx}
⟨001⟩	e_H-e_{001}	e_H-e_{001}	e_H+2e_{001}	0	0	0
⟨111⟩	e_H	e_H	e_H	e_{111}	e_{111}	e_{111}
⟨110⟩	$e_H+e_{001/2}$	$e_H+e_{001/2}$	e_H-e_{001}	0	0	$3e_{111/2}$

ence they have been listed in Table II. A straightforward calculation gives the results listed in Tables III, IV, and V.

III. EXPERIMENTAL DETAILS

A. Apparatus

All samples used in this work were cut from epitaxial layers of heavily doped GaP, kindly provided to us by Dr. Poiblaud from Radio Technique Compelec (Caen). The nitrogen concentration was in the area of 2×10^{18} cm^{-3} with a residual donor concentration of about 4×10^{16} cm^{-3}. The substrates were single-crystal slices of undoped GaP whose typical thickness was about 350 μm. Layers were grown on either the {001} or {110} faces of the substrate. This permitted us to cut long samples along the ⟨100⟩, ⟨110⟩, and ⟨111⟩ crystallographic directions which, after careful polishing of the two narrow pressure faces, were mounted between two optically flat pistons inside a liquid-helium cryostat. The details of the stress apparatus have been already described[14] and will not be repeated here. In order to resolve all possible components, the luminescence of our sample was pumped by the 5145-Å line of an Ar^+ ion laser, using a typical power of about 30 mW. In some cases, different families of exciton states superimpose in the experimental range but belong to nonequivalent orientations. In this case, a cw dye laser was pumped by the Ar^+ ion and used to identify the different families by standard selective excitation methods.[15]

B. Analysis of data

The luminescence spectra of nitrogen-doped GaP is a well-documented subject in the current literature, and numerous features, specific to both isolated and associated nitrogen-nitrogen atoms, have now been well established. For instance, Gil *et al.*[13] recently investigated the competing effects of local field and J-J coupling on the luminescence spectra of deep N-N pairs ($i<7$). They identified most components in terms of allowed (A-like, $J=1$) and forbidden (B-like, $J=2$) manifolds split by local-field effects. They found that the local perturbation experienced by the bound hole was mainly uniaxial and gave no evidence of the spatial orientation of NN_i pairs. This is because, the hole orbiting about 25 Å around the defect, the magnitude of the perturbation experienced in this case is too weak to split all possible components. Roughly speaking, this results only in a triplet structure, characterized by strong A_0, A_1, and B_1 components, which has long been recognized[2,14] and will not be discussed anymore.

In this work we focus on the bound-electron states. Since we want to probe their spatial degeneracy from uniaxial stress, we must concentrate on singlet components of the bound-exciton complex. This is done in the following way. Because of the degenerate structure of the topmost

TABLE III. Axial deformation experienced by the different families, constitutive defects, and degeneracy, under ⟨001⟩ stress.

Local symmetry	Axial deformation	Constitutive defects	Degeneracy	Symmetry in the stressed crystal
C_{3v}	e_H	(aaa), $(\bar{a}aa)$, $(a\bar{a}a)$, $(aa\bar{a})$	4	C_s
D_{2d}	$e_H-\frac{e_{001}}{3}$	$(a00)$, $(0a0)$	2	D_2
	$e_H+2\frac{e_{001}}{3}$	$(00a)$	1	D_{2d}
C_{2v}	e_H-e_{001}	$(aa0)$, $(a\bar{a}0)$	2	C_{2v}
	$e_H+e_{001/2}$	$(a0a)$, $(a0\bar{a})$, $(0aa)$, $(0a\bar{a})$	4	E
C_s	$e_H+\frac{2(c^2+a^2)}{2a^2+c^2}e_{001}$	(aac), $(aa\bar{c})$, $(a\bar{a}c)$, $(\bar{a}ac)$	4	C_s
	$e_H+\frac{a^2-c^2}{2a^2+c^2}e_{001}$	(aca), $(\bar{a}ca)$, $(a\bar{c}a)$, $(ac\bar{a})$, $(\bar{c}aa)$, $(c\bar{a}a)$, (caa), $(ca\bar{a})$	8	E
C_2	e_H-e_{001}	$(ab0)$, $(ba0)$, $(a\bar{b}0)$, $(b\bar{a}0)$	4	C_2
	$e_H+\frac{2b^2-a^2}{a^2+b^2}e_{001}$	$(a0b)$, $(0ab)$, $(\bar{a}0b)$, $(0a\bar{b})$	4	C_2
	$e_H+\frac{2a^2-b^2}{a^2+b^2}e_{001}$	$(b0a)$, $(b0a)$, $(0b\bar{a})$, $(0\bar{b}a)$	4	C_2
E	$e_H+\frac{2c^2-a^2-b^2}{a^2+b^2+c^2}e_{001}$	(abc), $(\bar{a}bc)$, $(a\bar{b}c)$, $(ab\bar{c})$, (bac), $(b\bar{a}\,\bar{c})$, $(b\bar{a}c)$, $(ba\bar{c})$	8	E
	$e_H+\frac{2a^2-b^2-c^2}{a^2+b^2+c^2}e_{001}$	(bca), $(\bar{b}ca)$, $(b\bar{c}a)$, $(bc\bar{a})$, (cba), $(\bar{c}ba)$, $(c\bar{b}a)$, $(cb\bar{a})$	8	E
	$e_H+\frac{2b^2-a^2-c^2}{a^2+b^2+c^2}e_{001}$	(acb), $(\bar{a}cb)$, $(a\bar{c}b)$, $(ac\bar{b})$, (cab), $(c\bar{a}b)$, $(ca\bar{b})$, $(\bar{c}ab)$	8	E

TABLE IV. Same as Table III but for a ⟨111⟩ stress.

Local symmetry	Axial deformation	Constitutive defects	Degeneracy	Symmetry in the stressed crystal
C_{3v}	e_H+2e_{111}	(aaa)	1	C_{3v}
	$e_H-\frac{2}{3}e_{111}$	$(aa\bar{a})$, $(a\bar{a}a)$, $(\bar{a}aa)$	3	C_s
D_{2d}	e_H	$(a00)$, $(0a0)$, $(00a)$	3	C_s
C_{2v}	e_H+e_{111}	$(aa0)$, $(a0a)$, $(0aa)$	3	C_s
	e_H-e_{111}	$(a\bar{a}0)$, $(a0\bar{a})$, $(0a\bar{a})$	3	C_s'
C_s	$e_H+2\frac{a^2+2ac}{2a^2+c^2}e_{111}$	(aac), (aca), (caa)	3	C_s
	$e_H-\frac{2a^2}{2a^2+c^2}e_{111}$	$(\bar{a}ac)$, $(\bar{a}ca)$, $(c\bar{a}a)$, $(a\bar{a}c)$, $(ac\bar{a})$, $(ca\bar{a})$	6	E
	$e_H+2\frac{a^2-2ac}{2a^2+c^2}e_{111}$	$(aa\bar{c})$, $(a\bar{c}a)$, $(\bar{c}aa)$	3	C_s'
C_2	$e_H+\frac{2ab}{a^2+b^2}e_{111}$	$(ab0)$, $(ba0)$, $(a0b)$, $(b0a)$, $(0ab)$, $(0ba)$	6	E
	$e_H-\frac{2ab}{a^2+b^2}e_{111}$	$(\bar{a}b0)$, $(b\bar{a}0)$, $(\bar{a}0b)$, $(b0\bar{a})$, $(0\bar{a}b)$, $(0b\bar{a})$	6	E
E	$e_H+2\frac{ab+bc+ac}{a^2+b^2+c^2}e_{111}$	(bca), (abc), (bac), (acb), (cab), (cba)	6	E
	$e_H+2\frac{ab-ac-bc}{a^2+b^2+c^2}e_{111}$	$(ab\bar{c})$, $(ba\bar{c})$, $(bc\bar{a})$, $(a\bar{c}b)$, $(\bar{c}ab)$, $(\bar{c}ba)$	6	E
	$e_H+2\frac{ac-ab-bc}{a^2+b^2+c^2}e_{111}$	$(b\bar{c}\,\bar{a})$, $(b\bar{a}\,\bar{c})$, $(\bar{a}b\bar{c})$, $(\bar{c}b\bar{a})$, $(\bar{a}\,\bar{c}b)$, $(\bar{c}\,\bar{a}b)$	6	E
	$e_H+2\frac{bc-ab-ac}{a^2+b^2+c^2}e_{111}$	$(bc\bar{a})$, $(cb\bar{a})$, $(\bar{a}bc)$, $(\bar{a}cb)$, $(b\bar{a}c)$, $(c\bar{a}b)$	6	E

valence band, the uniaxial stress first splits all $(A$-$B)$ manifolds in a series of A_1-like lines which shift toward high energy (they are associated with $|\frac{3}{2},\frac{3}{2}\rangle$ hole wave functions) and two series of A_0 and B_1 lines which shift to low energy. They are associated with $|\frac{3}{2},\frac{1}{2}\rangle$ hole wave functions. This corresponds to the stress-induced splitting of the valence band and gives three lines per nonequivalent site. Among these, two lines (A_0,B_1) appear mainly in luminescence experiments, one line (A_1) is best probed by luminescence excitation spectroscopy.[15] Moreover, in the range of uniaxial stress investigated in this work, the stress direction always provides a good quantization axis and the identification of A_0, A_1, and B_1 components is straightforward, with the help of polarized light.[16] All A_0-like lines appear mainly in polarization E parallel to the stress direction, while A_1 and B_1 appear in both parallel and perpendicular polarizations. Superimposed on this fine-structure splitting is the orientational splitting in which we are interested. It gives several series of B_1, A_0, and A_1 lines and comes only from the electron contribution. Consider, for instance, NN_1 under ⟨001⟩ stress, where we resolve two series of manifolds. Within one manifold, the energy separation A_0-B_1 originates only from the internal structure of the exciton and is constant versus stress. On the contrary, the orientational splitting A_0-$A_{0'}$ increases versus stress. Such a behavior can be qualitatively understood in terms of the axial deformation experienced by the electron wave function as already seen under hydrostatic pressure conditions:[17] the electron binding energy decreases when decreasing the nitrogen-nitrogen distance.

IV. RESULTS

A. NN_1 pairs

Under ⟨001⟩ stress, we find two families of A_0, A_1, and B_1 components. This is displayed in Fig. 1. As already stated, all A_0 $(J=1,\ M_J=0)$ and B_1 $(J=2,\ M_J=\pm1)$ excitonic states have been identified using the standard selection rules illustrated in Fig. 2. As usual, in the limit of large uniaxial stress (which means a good quantization axis), we find A_0-like components appearing in polarization $E\|X$ (π polarization) and B_1 states in polarization $E\perp X$ (σ polarization). Since only two families could be resolved, we deduce that NN_1 has a D_{2d}, C_{2v}, or C_s local symmetry. This is confirmed by inspection of the integrated intensity of the two luminescence lines which are indeed in the ratio 1:2.

Under ⟨111⟩ stress, we get for an external pressure of 500 bars two families with identical statistical weight. This is only found for defects with C_{2v} or C_2 symmetry. Since C_2 was already excluded from ⟨001⟩ stress experiments, we conclude that NN_1 has C_{2v} symmetry and that all nitrogen-nitrogen pairs are oriented along the $[aa0]$ or equivalent crystal directions.

TABLE V. Same as Table III but for ⟨110⟩ stress.

Local symmetry	Axial deformation	Constitutive defects	Degeneracy	Symmetry in the stressed crystal
C_{3v}	e_H+e_{111}	(aaa), $(aa\bar{a})$	2	C_s
	e_H-e_{111}	$(a\bar{a}a)$, $(\bar{a}aa)$	2	C_s'
D_{2d}	$e_H+e_{001/3}$	$(00c)$	1	C_{2v}
	$e_H-e_{001/6}$	$(c00)$, $(0c0)$	2	E
C_{2v}	$e_H+e_{001/2}+3e_{111/2}$	$(aa0)$	1	C_{2v}
	$e_H+e_{001/2}-3e_{111/2}$	$(a\bar{a}0)$	1	C_{2v}
	$e_H-e_{001/4}$	$(a0a)$, $(a0\bar{a})$, $(0aa)$, $(0a\bar{a})$	4	E
C_s	$e_H+\frac{a^2-c^2}{2a^2+c^2}e_{001}+\frac{3a^2}{2a^2+c^2}e_{111}$	(aac), $(aa\bar{c})$	2	C_s
	$e_H+\frac{a^2-c^2}{2a^2+c^2}e_{001}-\frac{3a^2}{2a^2+c^2}e_{111}$	$(a\bar{a}c)$, $(a\bar{a}\,\bar{c})$	2	C_s
	$e_H+\frac{1}{2}\frac{c^2-a^2}{2a^2+c^2}e_{001}+\frac{3ac}{2a^2+c^2}e_{111}$	(aca), $(ac\bar{a})$, $(ca\bar{a})$, (caa)	4	E
	$e_H+\frac{1}{2}\frac{c^2-a^2}{2a^2+c^2}e_{001}-\frac{3ac}{2a^2+c^2}e_{111}$	$(a\bar{c}a)$, $(a\bar{c}\,\bar{a})$, $(c\bar{a}a)$, $(c\bar{a}\,\bar{a})$	4	E
C_2	$e_H-e_{001}+\frac{3ab}{a^2+b^2}e_{111}$	$(ab0)$, $(ba0)$	2	C_2
	$e_H-e_{001}-\frac{3ab}{a^2+b^2}e_{111}$	$(\bar{a}b0)$, $(b\bar{a}0)$	2	C_2'
	$e_H+\frac{2b^2-a^2}{a^2+b^2}e_{001}$	$(a0b)$, $(a0\bar{b})$, $(0ab)$, $(0a\bar{b})$	4	E
	$e_H-\frac{2b^2-a^2}{a^2+b^2}e_{001}$	$(b0a)$, $(b0\bar{a})$, $(0ba)$, $(0b\bar{a})$	4	E
E	$e_H+\frac{1}{2}\frac{a^2+b^2-2c^2}{a^2+b^2+c^2}e_{001}+\frac{3ab}{a^2+b^2+c^2}e_{111}$	(abc), $(ab\bar{c})$, (bac), $(ba\bar{c})$	4	E
	$e_H+\frac{1}{2}\frac{a^2+b^2-2c^2}{a^2+b^2+c^2}e_{001}-\frac{3ab}{a^2+b^2+c^2}e_{111}$	$(a\bar{b}c)$, $(a\bar{b}\,\bar{c})$, $(b\bar{a}c)$, $(b\bar{a}\,\bar{c})$	4	E
	$e_H+\frac{b^2+c^2-2a^2}{a^2+b^2+c^2}e_{001}+\frac{3bc}{a^2+b^2+c^2}e_{111}$	(bca), $(bc\bar{a})$, $(cb\bar{a})$, (cba)	4	E
	$e_H+\frac{b^2+c^2-2a^2}{a^2+b^2+c^2}e_{001}-\frac{3bc}{a^2+b^2+c^2}e_{111}$	$(b\bar{c}a)$, $(b\bar{c}\,\bar{a})$, $(c\bar{b}a)$, $(c\bar{b}\,\bar{a})$	4	E
	$e_H+\frac{a^2+c^2-2b^2}{a^2+b^2+c^2}e_{001}+\frac{3ac}{a^2+b^2+c^2}e_{111}$	(acb), $(ac\bar{b})$, (cab), $(ca\bar{b})$	4	E
	$e_H+\frac{a^2+c^2-2b^2}{a^2+b^2+c^2}e_{0001}-\frac{3ac}{a^2+b^2+c^2}e_{111}$	$(a\bar{c}b)$, $(a\bar{c}\,\bar{b})$, $(c\bar{a}b)$, $(c\bar{a}\,\bar{b})$	4	E

Remember now that, under uniaxial stress, the change in nitrogen-nitrogen distance depends only on the pair orientation with respect to the stress direction. (See Tables III, IV, and V.) In the case of C_{2v} pairs under ⟨001⟩ stress, we expect the change in electron binding energy to decrease more slowly for the two defects perpendicular to the stress axis than for the four remaining ones. This is indeed what is found. In the experimental data obtained for NN_1 under ⟨001⟩ stress, we find an electron binding energy smaller for the heavy family (decreasing N-N distance) than for the light family (increasing nitrogen distance). In the case of ⟨111⟩ stress, we expect now the low energy A_0 line to correspond with the $[aa0]$ family, while for ⟨110⟩ stress, we should resolve three families: an A_0 line related to $[a\bar{a}0]$ pairs, an A_0'' line to $[aa0]$, then the four remaining configurations forming A_0'.

The three different families expected under ⟨110⟩ stress are indeed found by carefully examining the splitting pattern displayed in Fig. 1(c). Some accidental degeneracy of A_0' and B_1'' around 1 kbar complicates the data. This is best viewed on the luminescence excitation spectroscopy spectra displayed in Fig. 3. Setting the wavelength spectrometer on the low-energy peak B_1, we find, by varying the dye laser frequency, both A_0 and A_1 components which are associated with the first family. Turning now to B_1', we find again the features A_0' and A_1' which correspond to the second family. Lastly, setting the wavelength spectrometer to B_1'', we find A_0'' and A_1''. Of course, because of the near degeneracy of A_0' and B_1'',

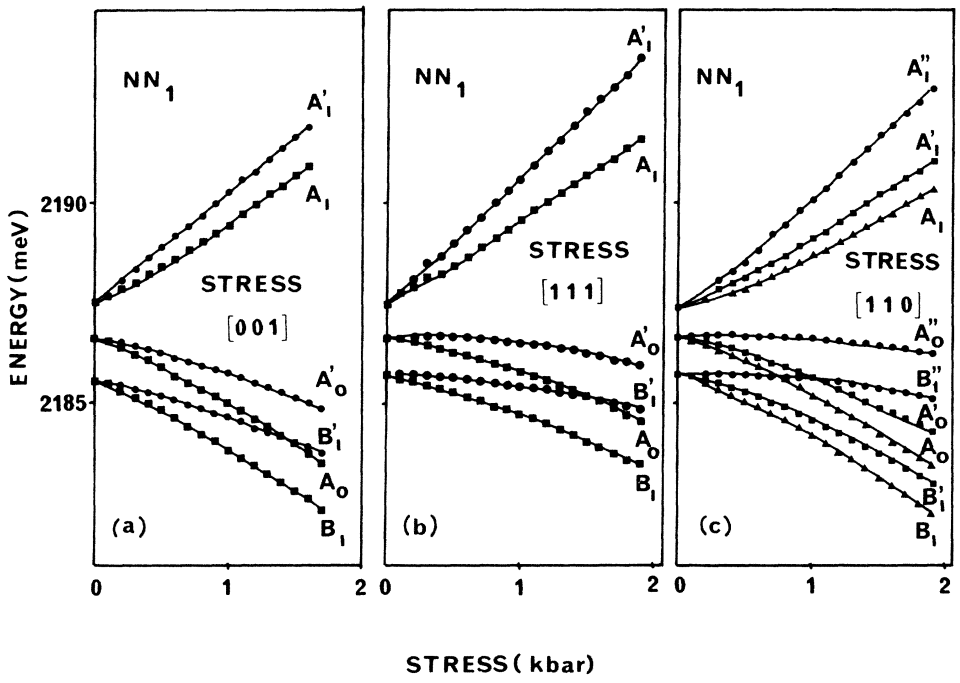

FIG. 1. Stress-induced splitting of NN_1 pairs under uniaxial stress. We resolve two different families under ⟨001⟩ stress, two families under ⟨111⟩ stress, and three families under ⟨110⟩ stress. All experiments have been performed at $T=2$ K.

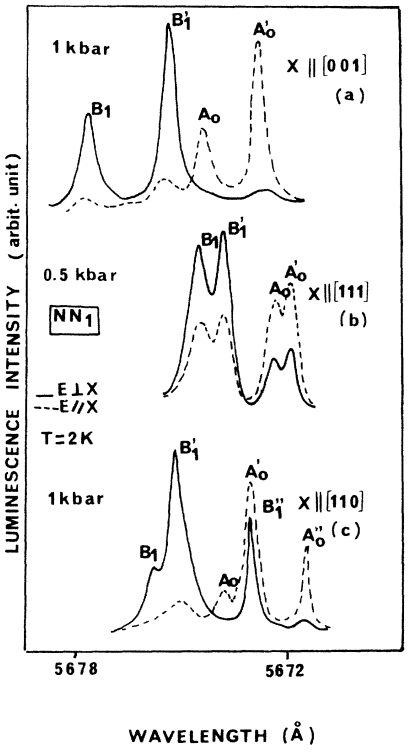

FIG. 2. Relative intensities and selection rules associated with the different families of NN_1 pairs at $T=2$ K. Solid lines: $\mathbf{E}\perp\hat{\mathbf{X}}$; broken lines: $\mathbf{E}\|\hat{\mathbf{X}}$.

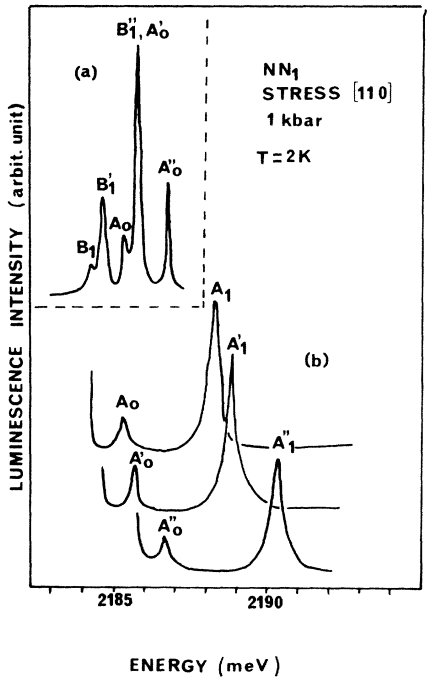

FIG. 3. Luminescence excitation of NN_1 pairs under 1 kbar pressure along the ⟨110⟩ direction. Inset: luminescence spectrum displaying all luminescence lines experimentally resolved.

a Raman spectrometer had to be used in order to separate the two lines.

B. NN_2 pairs

According to the classical assignment in Ref. 2, the local symmetry associated with NN_2 pairs should be D_{2d}. As a consequence, one expects to find (i) only two components under ⟨001⟩ stress—the respective intensities should be in a ratio 2:1, (ii) one single family under ⟨111⟩ stress, and (iii) again two families under ⟨110⟩ stress.

All results are summarized in Fig. 4. The most striking feature is that we resolve three different families under ⟨111⟩ stress. This cannot be accounted for within a D_{2d} symmetry but obviously involves a defect with lower point group. Consideration of Table II shows that only defects associated with orientations [*aac*] (local point group C_s) or [*abc*] (local point group E) give at least three families under ⟨111⟩ stress. The two possibilities can be discriminated by the different number of components induced under ⟨001⟩ and ⟨110⟩ stress.

In this case, we find two components under ⟨001⟩ stress, with respective intensity 1:2 (see inset in Fig. 4) and four components under ⟨110⟩ stress. This agrees well with a C_s symmetry and we conclude that NN_s traps in GaP correspond to pairs of nitrogen atoms substituted along crystal lines with equivalent [*aab*] orientations.

Since we have resolved the local symmetry of NN_2 pairs, we can go a little further and try to be more quantitative. In the case of ⟨001⟩ stress, the splitting pattern is close to the one already observed for NN_1. The high-energy transitions correspond to the heavy family and, in this case, the perturbation experienced along the pair axis should be a compression. On the contrary, it is expected to be a dilation for the second family of pairs. In view of the results listed in Table IV, such a situation is consistent with an [*aac*] orientation where $a > c$. In the limit where $a \gg c$, we should deal with a "C_s nearly C_{2v}" orientation and should resolve mainly two families with identical intensity under ⟨111⟩ stress. This is exactly what is found. At low energy we weakly separate two small components associated with [*aac*]- and [*aa$\bar{c}$*]-like families (A_0 and A_0', respectively) and, at much higher energy, we find one single component (two times more intense) associated with [*a$\bar{a}$c*]-like families.

Under ⟨110⟩ uniaxial stress, we expect and resolve four families. The corresponding ordering of levels should be [*a$\bar{a}$c*], [*a$\bar{c}$ $\bar{a}$*], [*aca*], and [*aac*] in order of increasing energy.

C. NN_3 pairs

Figure 5 summarizes the stress splitting pattern of NN_3 pairs. We find two different families under ⟨001⟩ stress, which indicates a symmetry C_{2v}, D_{2d}, or C_s. We next resolve three families under ⟨111⟩ stress, which gives a local field of C_s symmetry.

As concerns the relative intensity of the different pairs under ⟨001⟩ stress, the most populated family corresponds with the high-energy components (B_1',A_0',A_1') (see Fig. 6). Again we find a factor of 2 with respect to their counterparts (A_0,B_1) and the experimental spectrum closely resembles the one obtained for NN_1 and NN_2. Under ⟨111⟩ stress, the relative intensities are 1:1:2 and the higher intensity is associated with the high-energy components (A_1'',A_0'',B_1''). We do not resolve A_1 and A_1' components for the low-intensity pairs. Again we emphasize that the spectra closely correlate with the data observed for NN_2.

Now concerning ⟨110⟩ stress, we observe four families with a relative intensity of 2:2:1:1. The stress splitting

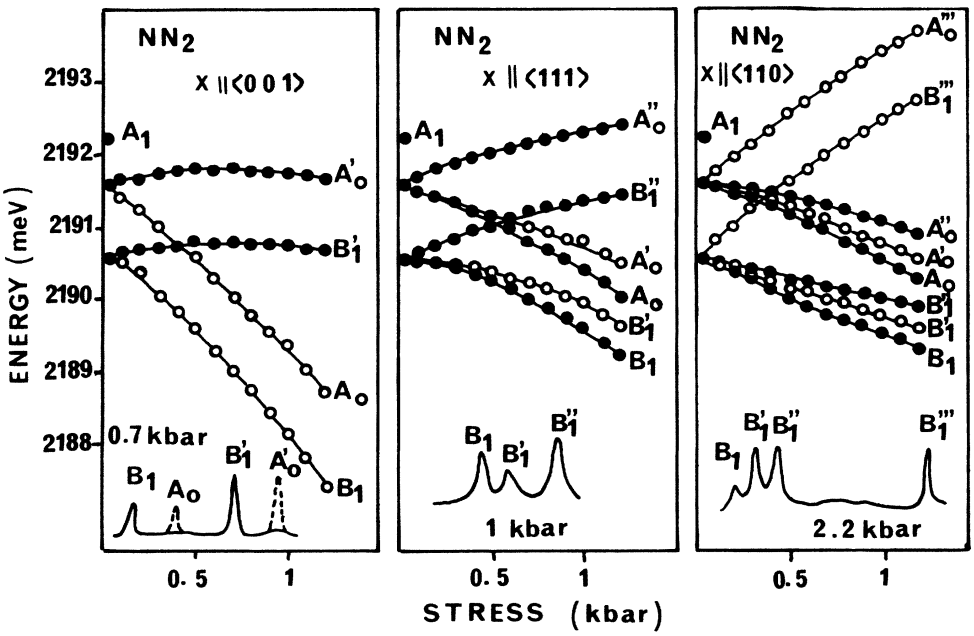

FIG. 4. Same as Fig. 1 but for NN_2. Inserted are typical luminescence spectra.

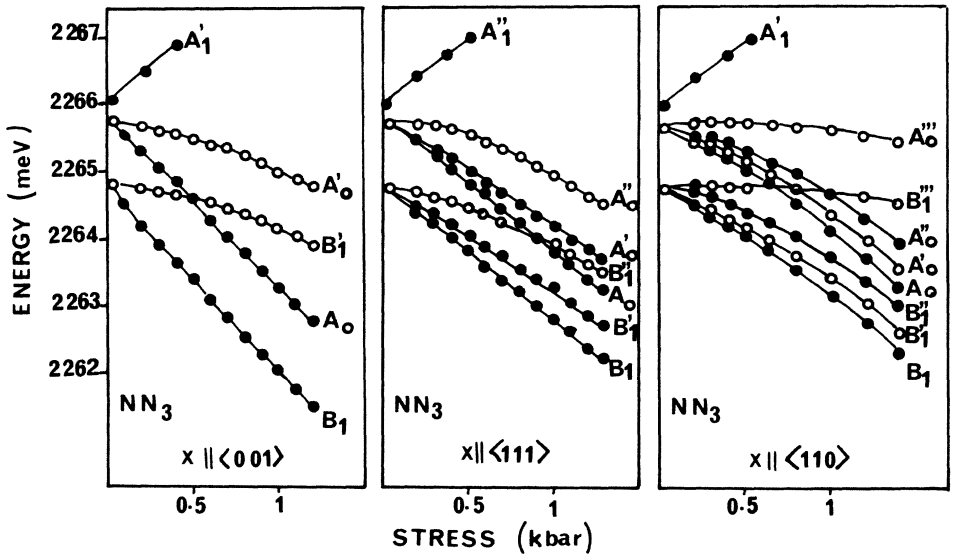

FIG. 5. Stress-induced splitting of NN_3 pairs under both ⟨001⟩ and ⟨111⟩ stress and ⟨110⟩ stress.

pattern is given in Fig. 5. The low-energy family corresponds to little shoulders hardly seen on the experimental spectra below 1 kbar but, increasing the pressure, we could resolve both A_0 and B_1 but not A_1. From the similarity of data between NN_2 and NN_3, we conclude that NN_3 corresponds to a C_s symmetry: [*aac*] pairs with $a > c$.

D. NN_4 pairs

We find results which closely resemble the data reported for NN_1. Under ⟨001⟩ stress we resolve two families of defects, the most important one lying at high energy. Under ⟨111⟩ stress we find again two families, but now both have identical intensity. Lastly, under ⟨110⟩ stress, we resolve three families whose relative intensities are in the ratio 4:1:1. This corresponds with C_{2v} symmetry and we conclude that both NN_1 and NN_4 pairs are oriented along the [*aa*0] crystal directions. All results are summarized in Fig. 7.

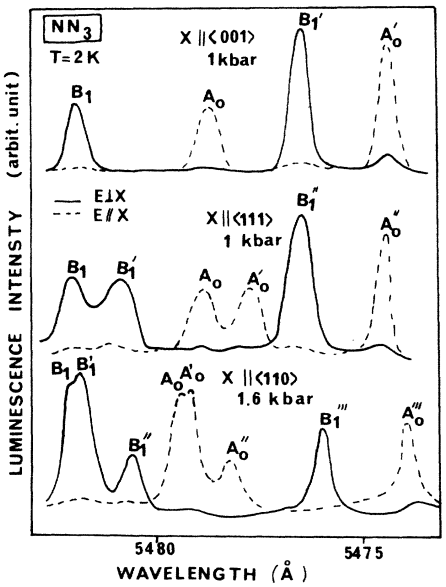

FIG. 6. Illustration of relative intensities and selection rules observed for NN_3.

E. NN_5 pairs

All experimental results are displayed in Fig. 8. We would expect, from the standard assignment of NN pairs, to find defects lying in the ⟨310⟩ direction and having C_2 symmetry. This is not what is found. According to Table II, we should find three different families under ⟨001⟩ stress. We find only two, with a rather large splitting and a factor of 2 in relative intensities. In a first approximation, this rules out the possibility of a C_2 type of defect and leaves only three possibilities: D_{2d}, C_{2v}, or C_s.

Finding the right assignment is not obvious. Consider first the fan diagrams displayed in Fig. 8. We resolve two families under ⟨111⟩ stress and three families under ⟨110⟩ stress, which, qualitatively speaking, reminds us of the splitting pattern already displayed for NN_1 and NN_4, and favor a C_{2v} symmetry. This is no longer true if we consider now the ordering and relative intensities of the different families.

Remember, that under ⟨001⟩ stress, both NN_1 and NN_4 were characterized by experimental spectra which displayed the most populated family at higher energy. See, for instance, Fig. 2 and compare with the experimental data inserted in Fig. 7. Concerning NN_5, we find just the opposite. Under ⟨111⟩ stress, we get a similar discrepancy. We would expect, according to the data collected for NN_1 and NN_4, to resolve two families with identical intensities (the same result would also be expected with a pure C_2-type defect) but this is not what is experimentally found. Deconvoluting the data with a Gaussian shape, we find a ratio of roughly 3:1 which is

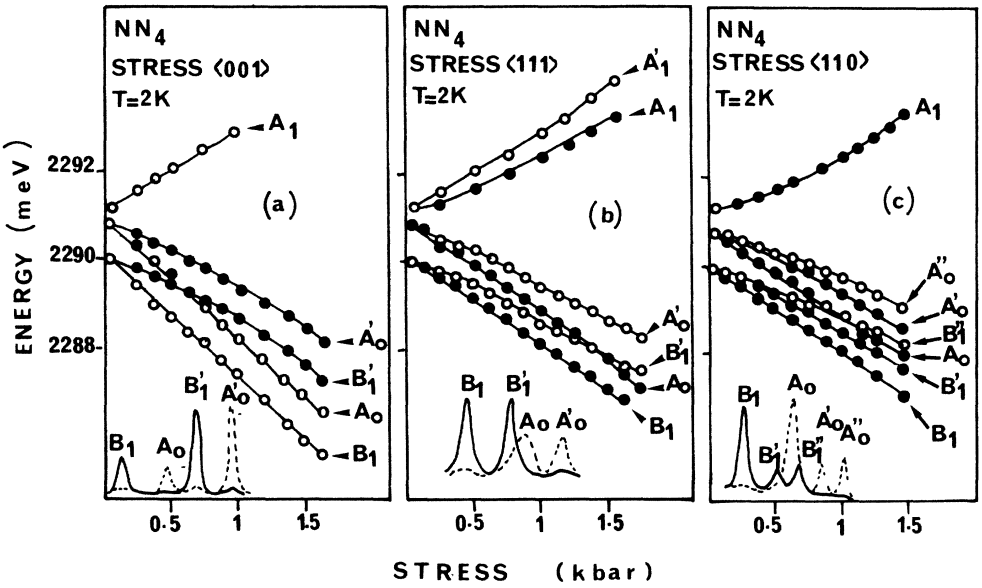

FIG. 7. Same as Fig. 1 but for NN_4. Inserted are typical luminescence spectra for different stress orientations.

not accounted for by the preceding symmetries and would correspond to a C_{3v} configuration. Lastly, considering the results collected under ⟨110⟩ stress, we find three lines with identical intensities which again cannot be directly accounted for by any of the D_{2d}, C_{2v}, or C_s symmetries (or even C_{3v} or C_2).

At this point of the discussion we are left with only two possibilities. One is that the defect symmetry is not axial so that it cannot be accounted for by the results listed in Tables III to V. The second is that we deal with some accidental degeneracy which makes some lines of the C_s manifold to mix and gives the experimental splitting pattern. In this case we would have a C_s type of defect [(aac) orientation of the pair axis] with $c > a$, in order to explain the larger sensitivity to ⟨001⟩ stress.

F. NN_6 and NN_7 pairs

Finally, let us consider NN_6 and NN_7. They lie very close in energy and, when we stress the crystal, some components of the different families cross. This gives additional features which complicate the interpretation of the data. Remember now that NN_6 should be associated, in the classification of Thomas and Hopfield, with defects of C_{3v} symmetry: we should not expect any stress-induced splitting under ⟨001⟩ stress. Again, this is not what is

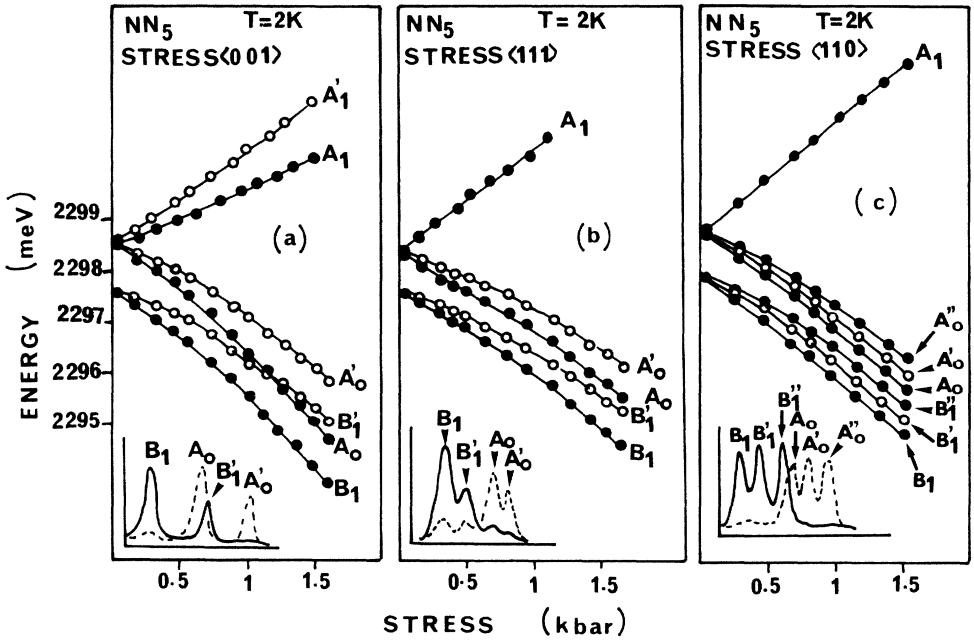

FIG. 8. Stress-splitting pattern of NN_5 pairs. Inserted are typical experimental spectra with about 1 kbar uniaxial stress.

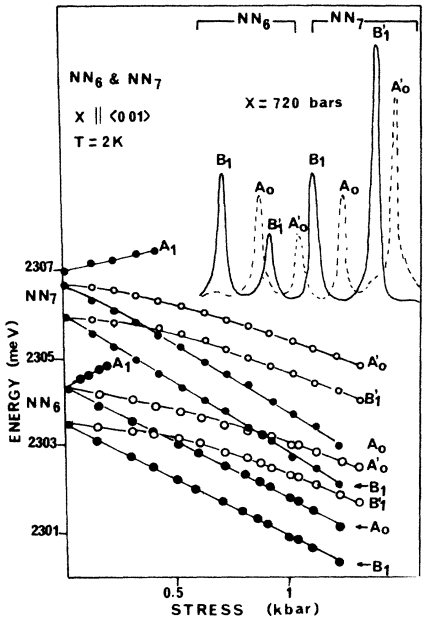

FIG. 9. Stress-induced splitting of NN_6 and NN_7 pairs under ⟨001⟩ stress.

found and it makes the discussion of NN_6 very interesting. For clarity we display in Fig. 9 the data collected under ⟨001⟩ stress. Figure 10 corresponds to ⟨111⟩ and ⟨110⟩ stress, respectively.

On the experimental spectra displayed in Fig. 9, we find two families of NN_6 pairs, which indicate a D_{2d}, C_{2v}, or C_s symmetry. The corresponding intensity ratio is 1:2 and the heavy component appears at low energy. Under ⟨111⟩ stress, we find again two components with relative intensities $\sim$1:2 and the heavy component appears also at low energy. Lastly, we find two components under ⟨110⟩ stress (1:2) but the heavy component appears at high energy. To summarize, we find that NN_6 cannot be associated with local fields of C_{3v} symmetry, but we find discrepancies similar to the one already noticed in the case of NN_5.

Concerning NN_7, the situation is quite different and all splitting patterns resemble the results noticed for NN_1 and NN_4. Accordingly, we believe that NN_7 corresponds with local fields of C_{2v} symmetry. We emphasize that, according to the standard assignment, NN_7 should be associated with a much lower local symmetry (132 pairs) and we do not believe that the discrepancy between our experimental findings and the theoretical predictions can be accounted for by accidental degeneracy.

V. CONCLUSION

The stress-splitting pattern, associated with NN_i pairs in GaP, has been investigated and the results discussed in terms of local symmetry groups associated with axial defects. The following conclusions have been drawn:

(i) In the case of pairs NN_1, NN_3, and NN_4, both the predicted (conventional) and experimental symmetries coincide. This is the only point of agreement between the standard views and our experimental findings.

(ii) In the case of pairs NN_2 and NN_6, we resolve more lines than we had expected. NN_2 can be easily associated with a C_s-type symmetry, while in the case of NN_6 the results appear much more controversial. This is a very puzzling point, especially in view of the conventional assignment which indicates for NN_6 a C_{3v} symmetry and was supported by magnetic field experiments[2] (see Table VI). To what extent this discrepancy can be accounted for by lattice relaxation or really question the conventional assignment is open to discussion and will be discussed in detail in the following paper.

(iii) In one case, NN_7, the conventional assignment corresponds to a very low symmetry group (E) which is not

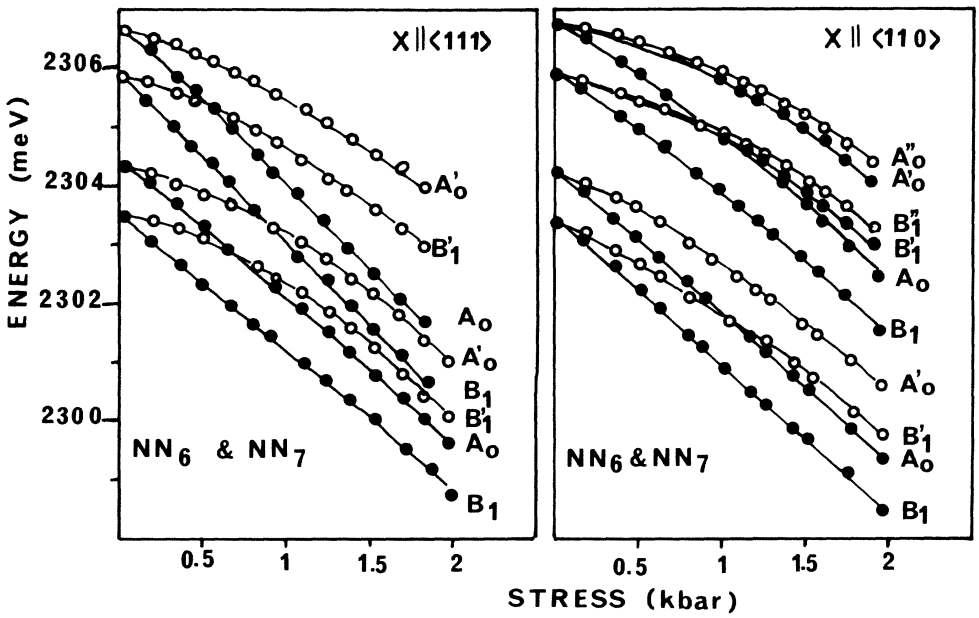

FIG. 10. Same as Fig. 9 but for ⟨111⟩ and ⟨110⟩ stress.

TABLE VI. Summary of the experimental results obtained in this work and in the work of Ref. 2. In parentheses we list the total number of components expected from the standard assignment. Magnetic field: total number of lines; stress: A_0 components only. Dashes denote no experimental data available and asterisks correspond to pairs with complicated nonuniaxial symmetry.

Assignment symmetry	NN_1 (110) C_{2v}	NN_2 (200) D_{2d}	NN_3 (211) C_s	NN_4 (220) C_{2v}	NN_5 (310) C_2	NN_6 (222) C_{3v}	NN_7 (321) E
Magnetic field[a]							
$B\|\|[001]$	11 (16)	–	–	–	–	8 (8)	–
$B\|\|[110]$	9 (24)	–	–	–	–	11 (16)	–
Stress[b]							
$X\|\|[001]$	2 (2)	2 (2)	2 (2)	2 (2)	2 (3)	2 (1)	2 (3)
$X\|\|[111]$	2 (2)	3 (1)	3 (3)	2 (2)	2 (2)	2 (2)	2 (4)
$X\|\|[110]$	3 (3)	4 (2)	4 (4)	3 (3)	3 (4)	2 (2)	3 (6)
Local field symmetry	C_{2v} ($aa0$)	C_s (aac) $a>c$	C_s (aac) $a>c$	C_{2v} ($aa0$)	*	*	C_{2v} ($aa0$)

[a]Reference 2.
[b]This work.

experimentally found. All experimental spectra are very similar to the one observed for NN_1 and NN_4 and support a C_{2v}-type symmetry. It is hard to believe that, in this case, a lattice relaxation might increase the local symmetry from E to C_{2v}. We believe that this is the strongest argument against the conventional assignment of NN_i pairs in GaP.

(iv) Lastly, in two cases, NN_5 and NN_6, we find data which can hardly be interpreted in terms of unrelaxed substitutional positions whatever the pair symmetry is. The larger sensitivity noticed for ⟨001⟩ stress suggests some correlation with ⟨001⟩ orientations.

[1]J. J. Hopfield, D. G. Thomas, and R. T. Lynch, Phys. Rev. Lett. **17**, 312 (1966).
[2]D. G. Thomas and J. J. Hopfield, Phys. Rev. **150**, 680 (1966).
[3]L. Canham, G. Davies, E. C. Lightowlers, and G. W. Blackmore, Physica **117-118B**, 119 (1983).
[4]B. Monemar, H. P. Gislason, P. J. Dean, and D. C. Herbert, Phys. Rev. B **25**, 7719 (1982).
[5]N. Holonyak, Jr., and M. H. Lee, in *Semiconductors and Semimetals*, edited by R. K. Willardson and A. C. Beer (Academic, New York, 1979), Vol. 14, p. 38.
[6]R. A. Faulkner, Phys. Rev. **175**, 991 (1968).
[7]E. Cohen and M. D. Sturge, Phys. Rev. B **15**, 1039 (1977).
[8]J. C. Phillips, Phys. Rev. Lett. **22**, 285 (1968).
[9]C. Benoit à la Guillaume, Physica **117-118B**, 105 (1983).
[10]W. T. Masselink and Yia-Chung Chang, Phys. Rev. Lett. **51**, 509 (1983).
[11]A. A. Kaplyanskii, Opt. Spectrosk. **16**, 329 (1964), and references therein.
[12]J. Morgan and T. N. Morgan, Phys. Rev. B **1**, 739 (1970).
[13]B. Gil, J. Camassel, P. Merle, and H. Mathieu, Phys. Rev. B **25**, 3987 (1982).
[14]J. Altier, J. Camassel, and H. Mathieu, *Proceedings of the International Conference on Measurements and Control "Meco,"* edited by M. H. Hanza (Acta, Zurich, 1977), p. 65.
[15]B. Gil, J. L. Thomas, L. Martin, J. Camassel, and J. Allegre, Solid State Commun. **53**, 723 (1985).
[16]H. Mathieu, L. Bayo, J. Camassel, and P. Merle, Phys. Rev. B **22**, 4834 (1980).
[17]B. Gil, M. Baj, J. Camassel, H. Mathieu, C. Benoit à la Guillaume, N. Mestres, and J. Pascual, Phys. Rev. B **29**, 3398, (1984).